Topological entanglement entropy in the quantum dimer model on the triangular lattice

Shunsuke Furukawa[1,2,*] and Grégoire Misguich[3]
[1]*Department of Physics, Tokyo Institute of Technology, Meguro-ku, Tokyo 152-8551, Japan*
[2]*Institute for Solid State Physics, University of Tokyo, Kashiwa 277-8581, Japan*
[3]*Service de Physique Théorique, CEA Saclay, 91191 Gif-sur-Yvette Cedex, France*
(Received 8 December 2006; revised manuscript received 21 April 2007; published 5 June 2007)

A characterization of topological order in terms of bi-partite entanglement was proposed recently [A. Kitaev and J. Preskill, Phys. Rev. Lett. **96**, 110404 (2006); M. Levin and X.-G. Wen, *ibid.* 96, 110405 (2006)]. It was argued that in a topological phase there is a universal additive constant in the entanglement entropy, called the topological entanglement entropy, which reflects the underlying gauge theory for the topological order. In the present paper, we evaluate numerically the topological entanglement entropy in the ground states of a quantum dimer model on the triangular lattice, which is known to have a dimer liquid phase with $\mathbb{Z}_2$ topological order. We examine the two original constructions to measure the topological entropy by combining entropies on plural areas, and we observe that in the large-area limit they both approach the value expected for $\mathbb{Z}_2$ topological order. We also consider the entanglement entropy on a topologically nontrivial "zigzag" area and propose to use it as another way to measure the topological entropy.

DOI: 10.1103/PhysRevB.75.214407 PACS number(s): 75.10.Jm, 03.65.Ud, 05.30.−d

I. INTRODUCTION

Exotic phenomena in quantum many-body systems are accompanied by nontrivial patterns of entanglement in ground-state wave functions. One useful measure of entanglement for a many-body state $|\Psi\rangle$ is the entanglement entropy S_Ω between a part Ω of the system and the rest of the system $\bar{\Omega}$. It is defined as the von Neumann entropy of the reduced density matrix ρ_Ω obtained by tracing out the degrees of freedom of $\bar{\Omega}$:

$$S_\Omega = -\mathrm{Tr}\rho_\Omega \ln \rho_\Omega, \quad \rho_\Omega = \mathrm{Tr}_{\bar{\Omega}}|\Psi\rangle\langle\Psi|. \tag{1}$$

It has been clarified in the past few years that some important properties of a quantum ground state are encoded in the size dependence of S_Ω. For a system with short-range correlations only, Ω and $\bar{\Omega}$ correlate only in the vicinity of the boundary separating them and thus the entanglement entropy scales with the size of the boundary (boundary law).[1] However, at a critical point with algebraically decaying correlations, the scaling of entanglement entropy exhibits a universal logarithmic correction characterizing the criticality. Specifically, in a one-dimensional quantum critical system described by a conformal field theory (CFT), the entanglement entropy shows a logarithmic scaling law with a coefficient determined by the central charge of the CFT.[2] In some two-dimensional quantum critical states, the entanglement entropy also contains a universal contribution, related to the geometry of the subsystem.[3]

Another type of nontrivial entanglement can exist in a system with topological order.[4,5] Such a system exhibits degenerate ground states separated from excited states by an energy gap, and this degeneracy, which depends on the topology of the entire system, cannot be ascribed to any type of conventional spontaneous symmetry breaking. Indeed, it has been demonstrated in some models that these degenerate ground states cannot be distinguished by any local observable.[6–8] Preskill[9] suggested that this degeneracy can be regarded as a global encoding of information reminiscent of quantum error-correcting codes and is a consequence of some long-distance entanglement. A characterization of this global entanglement was realized recently by Kitaev and Preskill (KP) (Ref. 10) and by Levin and Wen (LW).[11] It was argued that if Ω is a disk (in a two-dimensional system) with a smooth boundary of length L, the entanglement entropy scales as

$$S_\Omega = \alpha L - \gamma + \cdots, \tag{2}$$

where the ellipsis represents terms which are negligible in the limit $L \to \infty$. If the area Ω is not a disk and has m disconnected boundaries, the topological term $-\gamma$ in Eq. (2) is multiplied by m. While the coefficient α depends on the microscopic details of the system, γ is a universal constant characterizing topological order and was dubbed the topological entanglement entropy. Indeed, γ measures the so-called total quantum dimension $\mathcal{D}$ of topological order by $\gamma = \ln \mathcal{D}$. In the case of topological order described by a discrete Abelian gauge theory (e.g., $\mathbb{Z}_n$), $\mathcal{D}$ is equal to the number of elements in the gauge group. In general, it is difficult to separate the topological term $-\gamma$ from the boundary term in Eq. (2) because, on a lattice, the discrete nature of the boundary makes it difficult to define unambiguously the length L. To solve this, KP and LW found some ways to define γ by forming a linear combination of the entanglement entropies on plural areas sharing some boundaries, and cancelling the boundary terms out to leave the topological term. KP and LW illustrated this idea using effective field theories and exactly solvable models.

In this paper, we analyze the entanglement entropy in the quantum dimer model (QDM) on the triangular lattice[12] and examine the effectiveness of the proposal in numerical calculations of finite-size systems. This model is known to exhibit a dimer liquid phase with $\mathbb{Z}_2$ topological order in a finite interval in the parameter space.[12] We mainly consider the Rokhsar-Kivelson (RK) point,[13] where the ground-states are exactly known and where the calculation of reduced density

matrices (and thus entanglement entropy) amounts to counting the number of dimer coverings of the lattice satisfying some particular constraints. We calculate the topological entanglement entropy numerically, and compare the result with $\gamma=\ln 2$ expected for $\mathbb{Z}_2$ topological order.

We comment on related systems here. Kitaev's model[14] is known to be the simplest solvable model with $\mathbb{Z}_2$ topological order, and the entanglement entropy of this model has been analyzed rigorously in Refs. 11 and 15 and the value $\gamma=\ln 2$ for the topological entropy was confirmed. The solvable QDM (kagome lattice) of Ref. 16 can be mapped onto Kitaev's model on the honeycomb lattice, and thus its entanglement entropy can be analyzed in the same way. These models give elegant results, but are too ideal for discussing generic features of topological order because they have a strictly zero spin-spin (or dimer-dimer in the QDM) correlation length and are completely free of finite-size effects. In this sense, our analysis on the QDM on the triangular lattice is a step toward more realistic systems—though we mainly consider the exact RK ground states, they have a finite dimer-dimer correlation length and finite-size effects arise. In the same spirit but for another kind of topological order, the entanglement entropy of Laughlin wave functions was analyzed numerically in Ref. 17.

The paper is organized as follows. In Sec. II, we give the basic definitions and settings in our analysis. In Sec. III, we numerically analyze the properties of entanglement entropy in the QDM on the triangular lattice. Especially, we examine the two constructions of topological entanglement entropy proposed by KP and LW. Furthermore, we consider the entanglement entropy on a particular topologically nontrivial area and design another procedure to extract γ, which, for QDMs, turns out to give an accurate value even in relatively small systems. We then conclude in Sec. IV.

II. DEFINITIONS AND SETTINGS

A. Model

We consider the QDM on the triangular lattice defined by the Hamiltonian[12,13]

$$H = \sum_{\text{rhombi}} \left[-t \left(\left| \rangle\langle \right| + \text{h.c.} \right) + v \left(\left| \rangle\langle \right| + \left| \rangle\langle \right| \right) \right], \tag{3}$$

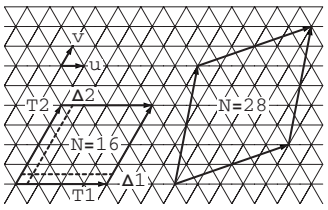

where the sum runs over all rhombi consisting of two neighboring triangles and we set $t>0$. At the Rokhsar-Kivelson (RK) point $v=t$, a ground-state is given exactly by the equal-amplitude superposition of all the dimer coverings[13]

$$|\text{RK}\rangle \equiv \frac{1}{\sqrt{|\mathcal{E}|}} \sum_{C\in\mathcal{E}} |C\rangle, \tag{4}$$

where $\mathcal{E}$ denotes the set of all the dimer coverings. This wave function exhibits exponentially decaying dimer-dimer correlations[12,18,19] and is an example of liquid with no broken symmetries.

This wave function is not the unique ground state if the lattice has a nontrivial topology (cylinder, torus, etc.). Let us

FIG. 1. Triangular lattices with periodic boundary conditions.

focus on the case of the torus hereafter. We draw two incontractible loops Δ_1 and Δ_2 which pass through the bonds and wind around the torus in x and y directions, respectively, as in Fig. 1. We classify $\mathcal{E}$ into four sets $\mathcal{E}^p$ with $p=++,+-,-+,--$, depending on the parity of the number of dimers crossing Δ_1 and Δ_2. The resultant sets $\mathcal{E}^p$, called topological sectors, are not mixed by any local dimer move (and thus by any term in the Hamiltonian). The spectrum of the Hamiltonian can therefore be determined separately in each sector. At the RK point, the ground state in each sector is given by

$$|\text{RK};p\rangle \equiv \frac{1}{\sqrt{|\mathcal{E}^p|}} \sum_{C\in\mathcal{E}^p} |C\rangle. \tag{5}$$

All these states have zero energy for the Hamiltonian (3) and span a four-dimensional ground-state manifold. It has been shown analytically and numerically that the degeneracy of the ground states and the exponential decay of the dimer-dimer correlation at the RK point persist in a finite range in the parameter space, forming a liquid phase with gapped excitations in $0.82(3)\lesssim v/t\leqslant 1$.[12,18,20,21] Decreasing v/t further, the model enters a valence bond crystal (VBC) phase with a large unit cell (12 sites), called $\sqrt{12}\times\sqrt{12}$ VBC.[12,21]

The ground-state degeneracy in the liquid phase indicates that this phase is topologically ordered. It is indeed a realization of the deconfined phase of a $\mathbb{Z}_2$ (Ising) gauge theory,[22] where the requirement that physical states must be invariant under gauge transformations is played by the dimer hard-core constraint and where the role of the gauge flux piercing a plaquette is played by a dimer-move operator around this plaquette.[16,23] The four ground-states correspond to the four possible choices to put (or not to put) a vortex through the two holes of the torus.

B. Lattice

The lattice is put on a torus and is defined by two vectors $\boldsymbol{T}_1$ and $\boldsymbol{T}_2$ specifying the periodicity. We mostly use lattices which are symmetric under 120° rotation, by setting

$$\boldsymbol{T}_1 = l\boldsymbol{u} + m\boldsymbol{v}, \quad \boldsymbol{T}_2 = -m\boldsymbol{u} + (l+m)\boldsymbol{v}, \tag{6}$$

where l and m are integers and $\boldsymbol{u}$ and $\boldsymbol{v}$ are unit vectors as shown in Fig. 1. The total number of sites is given by $N=l^2+lm+m^2$. The lattices we consider have $N=16,28,36,48,52,64$, which correspond, respectively, to $(l,m)=(4,0),(4,2),(6,0),(4,4),(6,2),(8,0)$. In Sec. III C, $N=100$ [corresponding to (10,0)] is also studied.

C. Reduced density matrix

To define a reduced density matrix (RDM) for the QDM, we must specify the local degrees of freedom of the model. To this end, we assign an Ising variable σ_k to each bond k of the lattice as in Ref. 23 and identify the presence/absence of a dimer on the bond as $\sigma_k=+1$ and -1, respectively. Any physical configuration $\{\sigma_k\}$ must satisfy the hard-core constraints: for each site of the lattice, there must be exactly one bond with $\sigma_k=1$ emanating from it. An area Ω is defined as a set of bonds. We define the matrix element of the RDM of a ground state $|\Psi\rangle$ as

$$\langle c_1|\rho_\Omega|c_2\rangle = \sum_{\bar{c}} \langle c_1,\bar{c}|\Psi\rangle\langle\Psi|c_2,\bar{c}\rangle, \tag{7}$$

where c_1 and c_2 are dimer configurations on Ω and the sum is over all the dimer configurations $\bar{c}$ on $\bar{\Omega}$. Note that we set $\langle c,\bar{c}|\Psi\rangle=0$ if $(c,\bar{c})$ is an unphysical configuration (violating the hard-core constraint).

Since the liquid phase under consideration exhibits degenerate ground states, we must specify for which state in the ground-state manifold we calculate the entanglement entropy. However, as long as the area is local, it was numerically demonstrated that the RDMs are identical for all states in the ground-state manifold, up to a correction which decays exponentially with the system size.[7] Thus in this case we can take any state in the ground-state manifold. At the RK point, which we mainly consider in the following, we simply take the "equal-amplitude" state (4). The RDM of the equal-amplitude state can be calculated in a way described in the Appendix, either by direct enumeration, or using Pfaffians.

III. NUMERICAL RESULTS

Here we present our numerical results. The idea of KP and LW should apply to the dimer liquid phase in $0.82(3) \lesssim v/t \leqslant 1$. The topological entropy for this phase is expected to be $\gamma=\ln 2 \simeq 0.6931$, reflecting $\mathbb{Z}_2$ topological order. We mainly consider the RK point $v/t=1$ with exact ground states (4) or (5), and calculate the entanglement entropies using the methods in the Appendix. For $v/t<1$, we perform Lanczos diagonalization of the Hamiltonian (3) for small systems (up to $N=36$), and calculate the entanglement entropies in the ground state.

A. Circular areas

We first consider the entanglement entropy on disks (areas with no holes) and discuss how the entanglement entropy scales with the extension of the area. Calculations were done for the RK wave function (4). As the choice of the area Ω, we define circular areas in the following way: we draw a circle with a radius R centered at a site or at an interior of a triangle and regard every bond whose midpoint is in the circle as an element of the area; see Fig. 2. This definition causes an unavoidable ambiguity in the radius R—different radii can result in the same area. For example, the possible radius for the smallest site-centered area (consisting of six bonds) ranges in $R_{\min}=0.5<R<\frac{\sqrt{3}}{2}=R_{\max}$. Here we analyze the data taking this ambiguity into account.

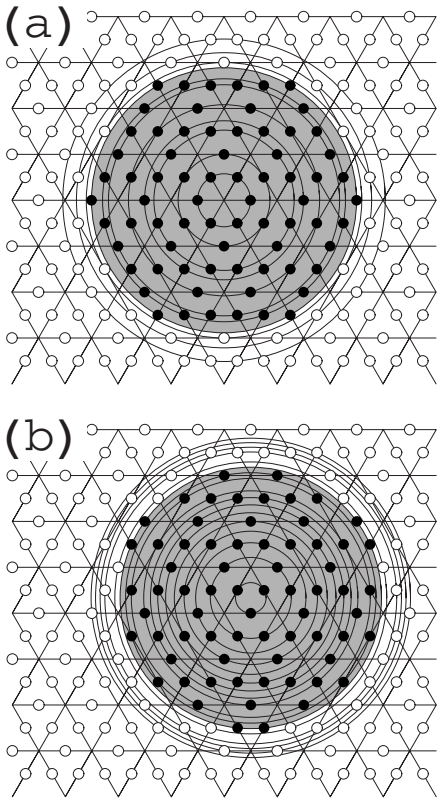

FIG. 2. Circular areas centered at (a) a site or (b) an interior of a triangle. As examples, areas with $R=2.5$ and $R=2.47$ are shaded for (a) and (b), respectively.

In Fig. 3, the values of S_Ω on circular areas are plotted versus the radius R. The different symbols correspond to different system sizes (from $N=16$ to 52) and a horizontal bar specifies the interval $[R_{\min},R_{\max}]$ ($N=52$ data points only, for clarity) The data from different system sizes almost coincide, showing the smallness of the finite-size effects. We fit

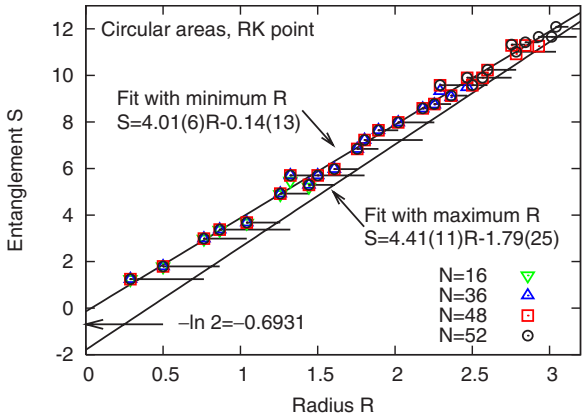

FIG. 3. (Color online) Entanglement entropy on circular areas with radii R at the RK point. The ambiguity in R is indicated by horizontal bars (only for $N=52$). The data for $N=52$ are fitted by lines using minimum or maximum radii. The resultant linear functions shown in the figure contains some numbers enclosed in parentheses, which indicates the standard errors in the last displayed digits.

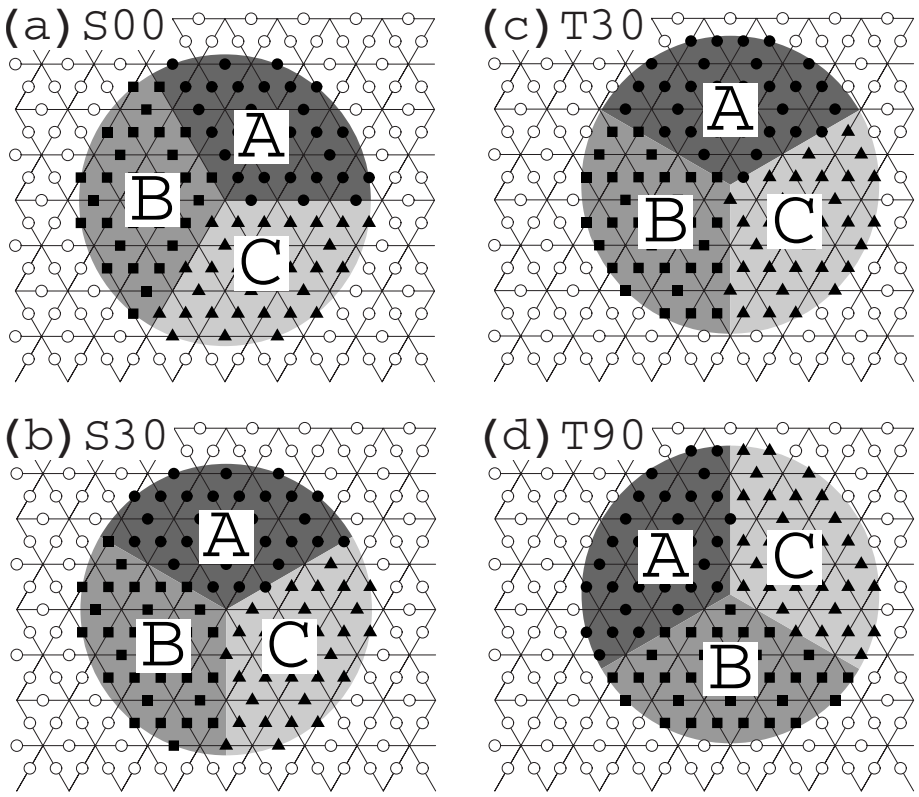

FIG. 4. Divisions of circular areas for the Kitaev-Preskill construction. (a) and (b): site-centered, $R=2.78$. (c) and (d): triangle-centered, $R=2.84$.

the data for $N=52$ by a linear relation using $R_{\min}$ or $R_{\max}$. We observe a rough agreement with the linear fitting in both cases as expected from the scaling form (2). The lines intersect the vertical axis around -0.1 and -1.8 when using $R_{\min}$ and $R_{\max}$, respectively. These values sandwich the expected value $-\ln 2 \simeq -0.6931$ but are both away from it. We also fitted the data separately for site-centered and triangle-centered cases (not shown in the figure), but no essential difference was observed. These results show that a direct check of the scaling (2) is difficult.

In general, on a lattice, the boundary of Ω is made of segments. If the sum of the segments is long enough, they contribute to the entanglement entropy by an amount proportional to the length. But in addition, we have to take into account the contribution coming from local correlations (between the regions Ω and $\bar{\Omega}$) taking place in the vicinity of the angles between successive segments. If Ω is large, the contribution from these angles may be small [of order $O(L^0)$, compared to the boundary length L], but this contribution will still be of the same order as the topological term we are looking for.

In the present case (circular areas), this ambiguity in defining a boundary length on the lattice appears as an ambiguity in the definition of R. To compute γ in a well-defined way, we need to turn to the constructions using plural areas, which we discuss in the next subsection.

B. Construction of the topological entropy using plural areas

KP and LW proposed two ways to extract the topological constant γ independently of the definition of the boundary length.[10,11] The idea is to evaluate γ by forming an appropriate linear combination of the entanglement entropies of different areas, so that the boundary contributions cancel out.

1. Kitaev-Preskill construction

In the KP construction,[10] we consider a circle and divide it into three "fans" A, B, and C. Then we form a linear combination

$$S_{\text{topo}}^{\text{KP}} = S_A + S_B + S_C - S_{AB} - S_{BC} - S_{CA} + S_{ABC}, \qquad (8)$$

where $S_{XY\cdots}$ denotes the entanglement entropy on a composite area $X \cup Y \cup \cdots$. In this combination, all the boundary contributions cancel out and a topological term $-\gamma$ should remain. For example, let us consider the line separating A and B. The boundary contributions along this line appears in S_A and S_B with a plus sign and in $-S_{BC}$ and $-S_{CA}$ with a minus sign. Some attention should be paid to the triple point, in the vicinity of which the areas have different shapes and thus possibly different local contributions. Three areas form a 120° angle: A, B, and C; three areas form a 240° angle: BC, AC, and AB. However, recalling that the entanglement entropies of an area and its complement are the same, the entropy of BC is equal to that of the complement of BC, which has the same shape with A in the vicinity of the triple point. Thus the *local* contributions from A and BC in the vicinity of the triple point should match. The same argument applies to every line and every corner, giving a cancellation of all the boundary contributions in Eq. (8). Assuming the scaling (2), we expect $S_{\text{topo}}^{\text{KP}} = -\gamma$ (for a large enough radius).

We apply this idea to the present model. We divide a circle by three lines emanating from the center as in Fig. 4. These lines are placed at angles $\theta_0 - 0$, $\theta_0 + 120° - 0$, and $\theta_0 + 240° - 0$ measured from the (reference) **u** direction. Here

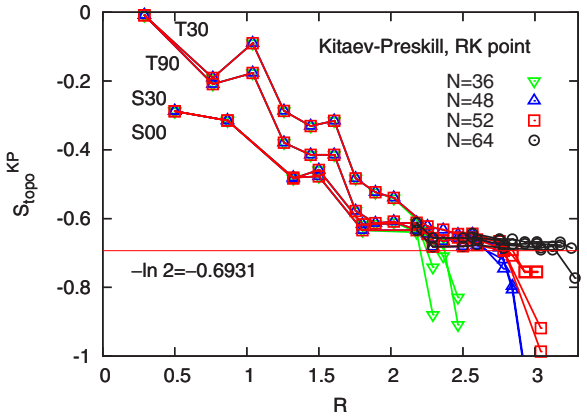

FIG. 5. (Color online) Topological entanglement entropy from the Kitaev-Preskill construction (8) at the RK point. Examples of areas are shown in Fig. 4. Some explicit values for large radii are shown in Table I.

"−0" represents an infinitesimal shift for avoiding collisions between the points (midpoints of bonds) and the boundaries. For example, points at an angle θ_0 belong to A, not to C. We take $\theta_0=0°$ or 30° for site-centered circles (referred to as "S00" and "S30") and $\theta_0=30°$ or 90° for triangle-centered circles ("T30" and "T90"). In these settings, the parts A, B, C are equivalent under 120° rotation, and we thus only need to calculate $S_{\text{topo}}^{\text{KP}}=3S_A-3S_{AB}+S_{ABC}$.

We first consider the case of the RK wave function (4). In Fig. 5, the data of $S_{\text{topo}}^{\text{KP}}$ are plotted versus the radii R of the circles. As in the case of circular areas presented in Fig. 3, finite-size effects are very small—except for the case where the circle ABC occupies a substantial part of the system, the data from different N's almost coincide. In the largest system $N=64$, we can regard the data up to $R\lesssim 3.1$ as good approximation to the values in the infinite system. In all the cases, $S_{\text{topo}}^{\text{KP}}$ decreases almost monotonically with R and for large radii (specifically, $2.2\lesssim R\lesssim 3.1$) shows values which are very close to $-\ln 2$ (see Table I), the expected value for a $\mathbb{Z}_2$ topologically ordered state.

Next we consider the region $v/t<1$ of the Hamiltonian (3). In $\mathbb{Z}_2$ liquid phase $0.82(3)\lesssim v/t\leqslant 1$, $S_{\text{topo}}^{\text{KP}}$ is expected to show $-\ln 2$ in the large-R limit. On the other hand, in $\sqrt{12}\times\sqrt{12}$ VBC phase $v/t\lesssim 0.82(3)$, where discrete symmetries are spontaneously broken, the finite-size ground-state can be approximated by a linear superposition of 12-fold symmetry-broken states. In such a state, we conjecture that the entanglement entropy on a disk Ω scales as $S_\Omega\simeq\alpha L+\ln d$ in the large-area limit, where d is the ground-state degeneracy and is equal to 12 in the present case. The constant term $\ln d$ is not topological in the sense that the same value would appear even if Ω had another geometry, unlike $-\gamma$ in Eq. (2). Note also that this constant is positive, in contrast to the negative topological term $-\gamma$. Assuming this, the combination (8) should give $\ln d$ in a symmetry-broken phase. Thus, $S_{\text{topo}}^{\text{KP}}$ is expected to jump from a negative (topological) value $-\ln 2$ to a positive (nontopological) value $\ln 12$ along with the transition from the liquid phase to the VBC phase. We performed Lanczos diagonalization of the Hamiltonian (3) for a lattice with $N=36$ (which is the maximum size in our exact diagonalization calculation and is compatible with $\sqrt{12}\times\sqrt{12}$ VBC ordering), and calculated $S_{\text{topo}}^{\text{KP}}$ in the ground-state, which lies in the sector $p=--$ in both the VBC and liquid phases on this lattice. The results are shown for two types of areas ("S00" and "T30") in Fig. 6. Because the system and area sizes are rather small, we do not observe a jump at the transition. However, we can already observe some tendency: for fixed v/t, $S_{\text{topo}}^{\text{KP}}$ tends to decrease as a

TABLE I. Some values of $-S_{\text{topo}}^{\text{KP}}$ at the RK point, divided by the expected value ln 2. The data for large radii are shown, and excellent agreement with the expectation can be seen.

	S00 case $-S_{\text{topo}}^{\text{KP}}/\ln 2$			T30 case $-S_{\text{topo}}^{\text{KP}}/\ln 2$	
Radius R	$N=52$	$N=64$	Radius R	$N=52$	$N=64$
2.18	0.9143	0.9143	2.57	0.9291	0.9283
2.29	0.9839	0.9835	2.75	0.9618	0.9513
2.50	0.9822	0.9822	2.84	0.9965	0.9518
2.60	0.9765	0.9760	2.93	1.0910	0.9635
2.78	1.0014	0.9897	3.01	1.0910	0.9635
3.04	1.3252	0.9967	3.18		0.9649
3.12		0.9967	3.25		0.9898

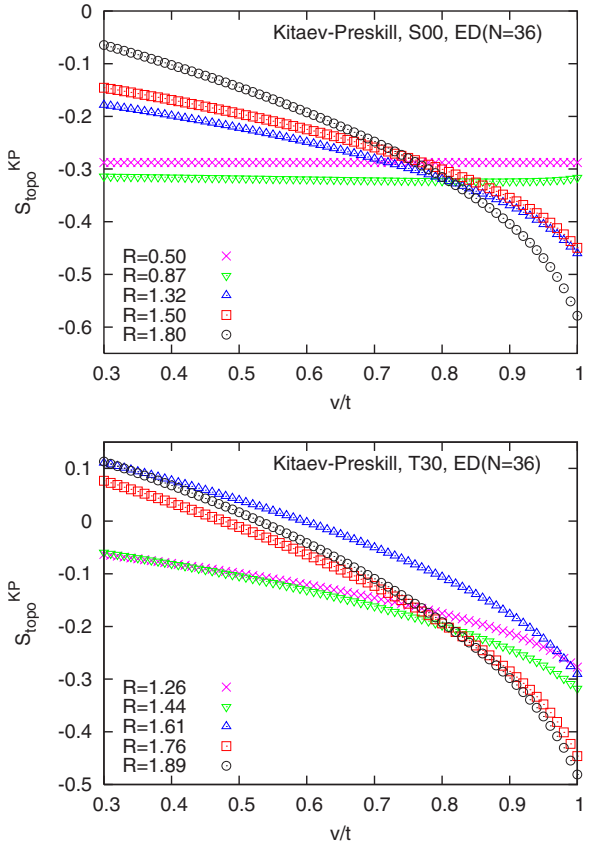

FIG. 6. (Color online) Kitaev-Preskill topological entropy (8) as a function of v/t for $N=36$. In the large-R limit, $S_{\text{topo}}^{\text{KP}}$ is expected to jump from $\ln 2$ in $\mathbb{Z}_2$ liquid phase $0.82(3)\lesssim v/t\leqslant 1$, to some positive value in the VBC phase $v/t\lesssim 0.82(3)$.

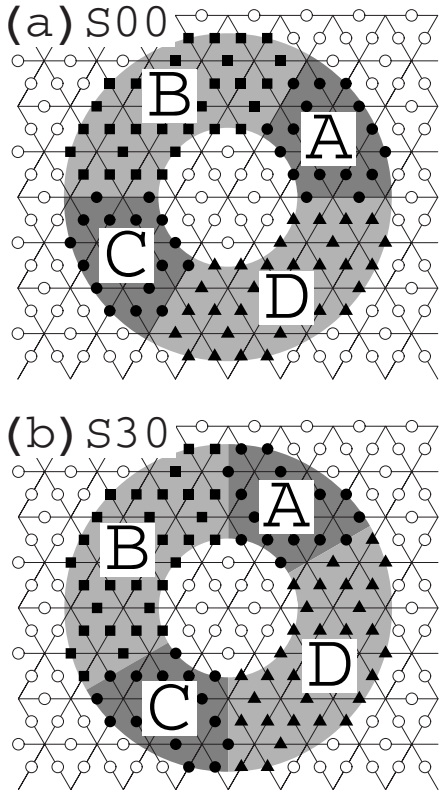

FIG. 7. Division of annular areas for the Levin-Wen construction.

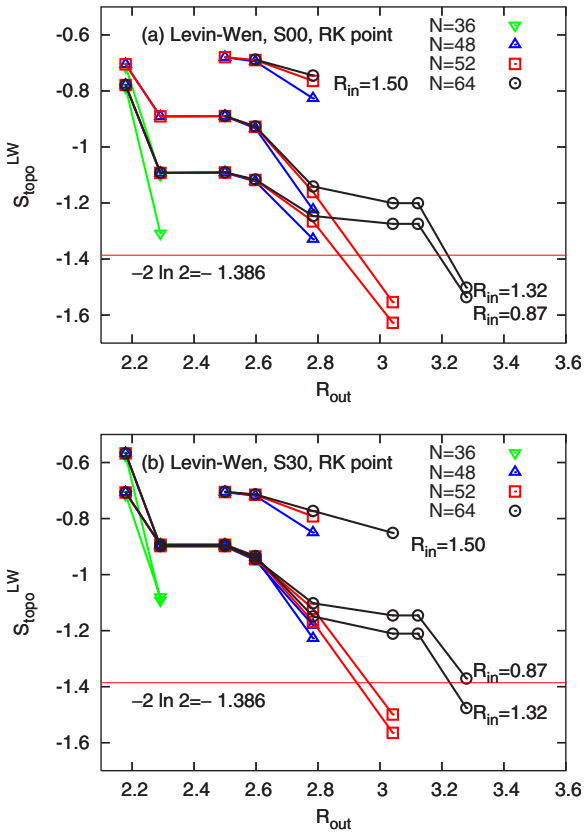

FIG. 8. (Color online) Topological entanglement entropy from the Levin-Wen construction.

function of R in the liquid side while it tends to increase in the VBC side. Some positive values of $S_{\text{topo}}^{\text{KP}}$ in the VBC phase are also seen in "T30" case.

2. Levin-Wen construction

In the LW construction,[11] we consider an annulus divided into four pieces as in Fig. 7, and form a combination

$$S_{\text{topo}}^{\text{LW}} = S_{ABCD} - S_{ABC} - S_{CDA} + S_{AC}. \tag{9}$$

This combination is guaranteed to be non-positive from the strong subadditivity inequality of entanglement entropies,[24] namely,

$$S_{\text{topo}}^{\text{LW}} = S_{X\cup Y} - S_X - S_Y + S_{X\cap Y} \leqslant 0, \tag{10}$$

where $X=A\cup B\cup C$ and $Y=C\cup D\cup A$. The combination (9) is expected to give -2γ for a topological phase and zero for a conventional phase (disordered, or with some symmetry-breaking order).

In Fig. 7, an annulus is divided by four lines at angles θ_0-0, $\theta_0+60°+0$, $\theta_0+180°-0$, $\theta_0+240°+0$. We consider only site-centered annuli, and we set $\theta_0=0°$ or 30° (again referred to as "S00" and "S30"). The result for the RK wave function is shown in Fig. 8. R_{in} and R_{out} denote the inner and outer radii of the annulus respectively, and $S_{\text{topo}}^{\text{LW}}$'s are plotted as a function of R_{out}. Up to $R_{\text{out}}\lesssim 3.1$, where the data for $N=64$ well approximate the values in the infinite system, we observe that $S_{\text{topo}}^{\text{LW}}$ monotonically decreases with R_{out} and approaches $-2\ln 2$. Unfortunately, the convergence to $-2\ln 2$ is not very clear up to this radius. In the LW construction, the requirement for the convergence is $\xi \ll R_{\text{in}}$, $R_{\text{out}}-R_{\text{in}}$, $L-2R_{\text{out}}$, where ξ is the correlation length ($\simeq 1$ at RK point) and $L=\sqrt{N}$ is the linear system size (or equivalently, the maximum possible $2R_{\text{out}}$). Thus, the LW construction suffers from stronger finite-*area* (not finite-N) effects than the KP construction which just requires $\xi \ll R$, $L-2R$.

C. Zigzag area

We design a different way to evaluate γ using a thin "zigzag" area Ω winding around the torus as in Fig. 9. This area is invariant by translation in the x direction and all points (black circles in Fig. 9) are equivalent by symmetry. In contrast to the more complicated areas considered before, we expect the boundary (i.e., nontopological) contribution to S_Ω

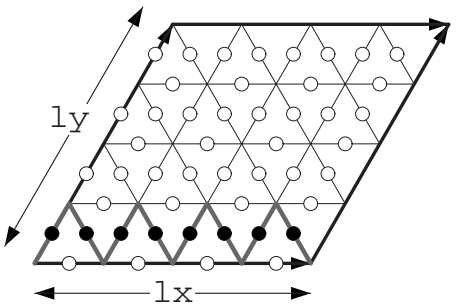

FIG. 9. Zigzag area on a lattice with $T_1=l_x\mathbf{u}$ and $T_2=l_y\mathbf{v}$.

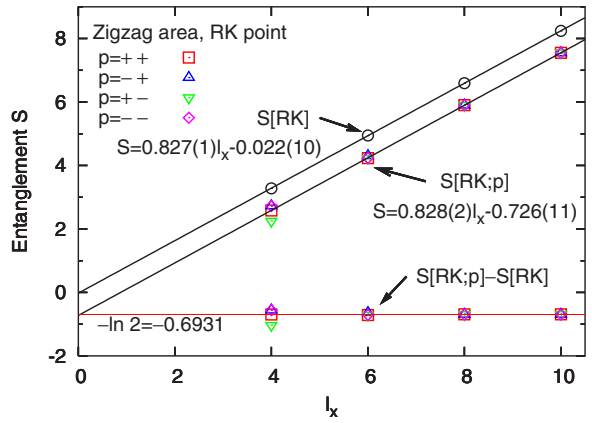

FIG. 10. (Color online) Entanglement entropies on a zigzag area at the RK point. The upper line is a linear fit to $S[\mathrm{RK}]$. The lower one is a fit to $S[\mathrm{RK};p=++]$ when $l_x=l_y$ is a multiple of 4 and $S[\mathrm{RK};p=--]$ otherwise. The topological constant estimated from the latter fit is $\gamma=0.73\pm0.01$. This particular choice of p as a function of l_x is motivated by the fact that, when $v/t<1$, it corresponds to the ground-state sector. Explicit values of $S[\mathrm{RK}]-S[\mathrm{RK};p]$ are shown in Table II.

to be precisely proportional to l_x, when l_x is sufficiently larger than the correlation length ξ. In this new geometry, the thermodynamic behavior is obtained as soon as $\xi \ll l_x$, l_y, whereas the KP construction requires $\xi \ll R$, $L-2R$, which is difficult to reach in exact diagonalization up to $N=36$. Since the area is topologically nontrivial (it contains the incontractible cut Δ_1), the value of S_Ω depends on the choice of the ground state, even for large systems. We calculate the entanglement entropies on this area in the ground-states $|\mathrm{RK}\rangle$ and $|\mathrm{RK};p\rangle$ on isotropic lattices $l_x=l_y$, and write them as $S[\mathrm{RK}]$ and $S[\mathrm{RK};p]$ respectively. The results are plotted in Fig. 10. As anticipated, S_Ω appears to be almost perfectly linear in l_x (compared with the results of Fig. 3). Moreover, we observe that the topological constant γ can be extracted in two different ways: (a) by extrapolating (through a linear fit) $S[\mathrm{RK};p]$ at "$l_x=0$" or (b) by $-\gamma \simeq S[\mathrm{RK};p]-S[\mathrm{RK}]$. These two follow from the scaling forms

$$S = \alpha_1 l_x \quad \text{for } |\mathrm{RK}\rangle,$$

$$S = \alpha_1 l_x - \gamma \quad \text{for } |\mathrm{RK};p\rangle, \tag{11}$$

where α_1 is a nonuniversal constant. A similar scaling was obtained rigorously by Hamma *et al.*[15] for a "ladder" area in Kitaev's model on the square lattice. Here we confirmed that it holds accurately even in a system with a finite correlation length. The scaling forms (11) provide an accurate way to calculate the topological constant γ even in relatively small systems. The condition (satisfied by QDM) is that topological sectors must be well defined and not mixed by the Hamiltonian, so that one can label the ground-states by their sectors. Computing γ from the largest system ($l_x=l_y=10$) gives our best estimate of the topological entanglement entropy $S[\mathrm{RK}]-S[\mathrm{RK};p=--]=0.6939$ (to be compared with $\ln 2=0.6931$); see Table II.

TABLE II. Values of $S[\mathrm{RK}]-S[\mathrm{RK};p]$ on a zigzag area, divided by ln 2. The sector p used in Fig. 10 is indicated by an asterisk, and gives the best estimate in most cases.

	$(S[\mathrm{RK}]-S[\mathrm{RK};p])/\ln 2$			
$l_x(=l_y)$	$++$	$-+$	$+-$	$--$
4	1.0024*	0.8051	1.4910	0.8051
6	1.0315	0.9248	1.0315	1.0212*
8	0.9944*	1.0022	1.0017	1.0022
10	0.9981	1.0028	0.9981	1.0011*

As another application, we use the scaling forms (11) to evaluate the topological term $-\gamma$ in the region $v/t<1$. We performed Lanczos diagonalization for lattices with $l_x=l_y=4$ and $l_x=l_y=6$. For $v/t<1$, the ground-state lies in the sector $p=++$ for $l_x=4$ and $p=--$ for $l_x=6$. We therefore compute the entropies $S[p=++;l_x=4]$ and $S[p=--;l_x=6]$ on the zigzag areas and approximate the topological term $-\gamma$ by a linear extrapolation to "$l_x=0$." In the thermodynamic limit, the constant term extracted in this way is expected to jump from $-\ln 2$ to a positive value, as in the case of Fig. 6. However, the $\sqrt{12}\times\sqrt{12}$ VBC ordering is compatible only with lattices where $l_x=l_y$ is a multiple of 6, and a linear relation $S_\Omega \simeq \alpha_1 l_x + \ln d$ holds only for such lattices.[27] The lattice with $l_x=l_y=4$ is thus out of this scaling, and the present estimation of the constant term is invalid for the VBC phase. Still, it can be used in the liquid phase. The result is shown in Fig. 11. A value close to ln 2 is recovered at the RK point but it decreases smoothly when decreasing v/t. No clear signature of a transition out of the topological liquid can be seen. Larger system sizes are probably required to locate the transition with this method. The problem probably lies in a rapid increase of the dimer-dimer correlation length (and thus stronger finite-size effects) when moving away from the RK point in the direction of the VBC phase.

IV. SUMMARY AND CONCLUSIONS

The concept of topological entanglement entropy was recently introduced by KP and LW as a way to detect and characterize topological order from a ground-state wave

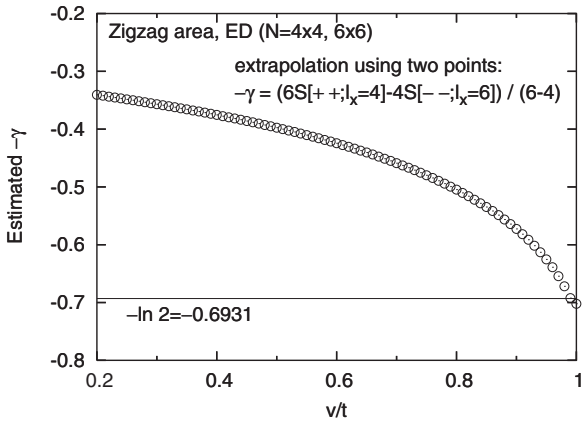

FIG. 11. The topological term $-\gamma$ as a function of v/t, estimated by using zigzag areas for $l_x=4$ and 6.

function. We have illustrated numerically how this approach works in the case of the $\mathbb{Z}_2$ liquid phase of the QDM on the triangular lattice. We found that, due to lattice discretization, the topological entropy γ cannot be obtained from a direct fit to the scaling form $S \simeq \alpha L - \gamma$. Instead, it is necessary to combine the entropies on plural areas to cancel out the boundary contributions, as suggested by KP and LW. In particular, for the KP construction, we clearly observed that in the large-area limit the topological entanglement entropy converges to $-\ln 2$ expected for $\mathbb{Z}_2$ topological order. We also proposed a procedure to evaluate the topological entropy using a topologically nontrivial "zigzag" area, which gives an accurate value even in small systems. For a system of linear size $l_x=10$, the later method provided an estimate of the topological entanglement entropy 0.6939 at the RK point, in remarkable agreement with the expected value ($\ln 2 = 0.6931$).

In addition to illustrating the concept of topological entanglement entropy in a "realistic" model, the present analysis offers an evidence of $\mathbb{Z}_2$ topological order in the QDM on the triangular lattice from a new perspective. Although the existence of topological degeneracy,[12] the analogy between this model and a $\mathbb{Z}_2$ gauge theory[23] and the absence of *any* broken symmetry[7] were already known, the present work confirms the $\mathbb{Z}_2$ structure in the ground-state wave function itself.

ACKNOWLEDGMENTS

The authors are grateful to C. Lhuillier, M. Oshikawa, and V. Pasquier for valuable discussions from the early stage of this work and for critical reading of the manuscript. S.F. thanks S. Ryu for useful discussions. The authors also acknowledge insightful comments from anonymous referees, which helped the authors to reexamine the calculations and to improve the manuscript with refined results. Most of this work was done while S.F. was at CEA Saclay and at Université P. & M. Curie (Paris), under the support of an exchange program "Collège Doctoral Franco-Japonais" and S.F. is thankful for the kind hospitality there. S.F. was also supported by a 21st Century COE Program at Tokyo Tech, "Nanometer-Scale Quantum Physics" from the MEXT of Japan.

APPENDIX: REDUCED DENSITY MATRIX OF THE RK WAVE FUNCTION

In this appendix, we derive a simple expression for the RDM of the RK wave function (4), and describe two methods for calculating it. A dimer configuration C on the entire system can be divided into the configurations on Ω and $\bar{\Omega}$:

$$C \in \mathcal{E} \to c \in \mathcal{E}_\Omega, \quad \bar{c} \in \mathcal{E}_{\bar{\Omega}}, \tag{A1}$$

where $\mathcal{E}_\Omega$ ($\mathcal{E}_{\bar{\Omega}}$) denote the set of all the possible dimer configurations on Ω ($\bar{\Omega}$). Now we consider the inverse mapping: given $c \in \mathcal{E}_\Omega$ and $\bar{c} \in \mathcal{E}_{\bar{\Omega}}$, under what condition is $(c,\bar{c})$ a physical configuration? This condition is given in terms of "occupied sites" of dimer configurations as follows. For a

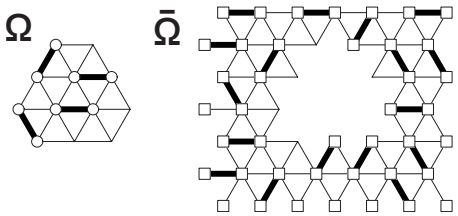

FIG. 12. Left (right): dimer configuration c ($\bar{c}$) on Ω ($\bar{\Omega}$) and their "occupied sites" $\Lambda(c)$ [$\Lambda(\bar{c})$], marked with circles (squares). In this picture, $\Lambda(c)$ and $\Lambda(\bar{c})$ are compatible and thus $(c,\bar{c})$ is physical.

configuration $c \in \mathcal{E}_\Omega$, we define $\Lambda(c)$ as the set of all the sites occupied by dimers in c, as shown in Fig. 12. We similarly define $\Lambda(\bar{c})$ for $\bar{c} \in \mathcal{E}_{\bar{\Omega}}$. In order for $(c,\bar{c})$ to be physical, (a) $\Lambda(c)$ and $\Lambda(\bar{c})$ should not overlap with each other and (b) the sum of $\Lambda(c)$ and $\Lambda(\bar{c})$ should cover all the sites of the lattice. Then we can rewrite the wave function (4) as

$$|\mathrm{RK}\rangle = \frac{1}{\sqrt{|\mathcal{E}|}} \sum_{\substack{c \in \mathcal{E}_\Omega, \bar{c} \in \mathcal{E}_{\bar{\Omega}} \\ \Lambda(c) \sqcup \Lambda(\bar{c}) = X_s,}} |c\rangle |\bar{c}\rangle, \tag{A2}$$

where X_s is the set of all the sites. If we list up all the possible $\Lambda(c)$ and write them as Λ_i $(i=1,2,\ldots)$, we can divide the summation as

$$|\mathrm{RK}\rangle = \frac{1}{\sqrt{|\mathcal{E}|}} \sum_i \sum_{\substack{c \in \mathcal{E}_\Omega \\ \Lambda(c)=\Lambda_i,}} |c\rangle \sum_{\substack{\bar{c} \in \mathcal{E}_{\bar{\Omega}} \\ \Lambda(\bar{c})=X_s \setminus \Lambda_i.}} |\bar{c}\rangle. \tag{A3}$$

We introduce

$$\mathcal{E}_\Omega^i \equiv \{c \in \mathcal{E}_\Omega | \Lambda(c) = \Lambda_i\},$$

$$\mathcal{E}_{\bar{\Omega}}^i \equiv \{\bar{c} \in \mathcal{E}_{\bar{\Omega}} | \Lambda(\bar{c}) = X_s \setminus \Lambda_i\}, \tag{A4}$$

and we define normalized states on Ω and $\bar{\Omega}$ as

$$|\psi_\Omega^i\rangle \equiv \frac{1}{\sqrt{|\mathcal{E}_\Omega^i|}} \sum_{c \in \mathcal{E}_\Omega^i} |c\rangle, \quad |\psi_{\bar{\Omega}}^i\rangle \equiv \frac{1}{\sqrt{|\mathcal{E}_{\bar{\Omega}}^i|}} \sum_{\bar{c} \in \mathcal{E}_{\bar{\Omega}}^i} |c\rangle. \tag{A5}$$

Then we arrive at the Schmidt decomposition

$$|\mathrm{RK}\rangle = \sum_i \sqrt{\lambda_i} |\psi_\Omega^i\rangle |\psi_{\bar{\Omega}}^i\rangle, \quad \text{with } \lambda_i \equiv \frac{|\mathcal{E}_\Omega^i| \cdot |\mathcal{E}_{\bar{\Omega}}^i|}{|\mathcal{E}|}. \tag{A6}$$

The RDM of this state reads

$$\rho_\Omega = \mathrm{Tr}_{\bar{\Omega}} |\mathrm{RK}\rangle\langle\mathrm{RK}| = \sum_i \langle \psi_{\bar{\Omega}}^i | \mathrm{RK}\rangle\langle \mathrm{RK} | \psi_{\bar{\Omega}}^i \rangle = \sum_i |\psi_\Omega^i\rangle \lambda_i \langle \psi_\Omega^i|. \tag{A7}$$

This expression is already diagonal and the λ_i's are the eigenvalues of ρ_Ω. The entanglement entropy is then given by $S_\Omega = -\Sigma_i \lambda_i \ln \lambda_i$. Since λ_i's are expressed using the number of dimer coverings for a given set of occupied sites, the task has been reduced to counting dimer coverings. This can be done

by direct enumeration using a recursive algorithm or by a Pfaffian method.

The Pfaffian method uses the fact that the number of dimer coverings is given by the the Pfaffian of an adjacency matrix with appropriate signs (entries are ±1 if the two sites are connected, and 0 otherwise).[25] Counting only configurations (c,c') such that $\Lambda(c)=\Lambda_i$ and $\Lambda(\bar{c})=X\backslash\Lambda_i$ can be done by removing some bonds of the lattice (setting to zero the corresponding matrix element): if a site x belongs to Λ_i, there cannot be any dimer between x and a site y if (xy) is not a bond of Ω. In the same way, any bond $(xy)\in\Omega$ involving a site $x\notin\Lambda_i$ must be switched off. The product $|\mathcal{E}^i_\Omega|\cdot|\mathcal{E}^i_{\bar{\Omega}}|$ is thus obtained from the Pfaffian of the modified adjacency matrix above.[28] It is clear that sites in the "bulk" of Ω are necessarily included in all Λ_i (otherwise the number of configurations is zero) and those in the bulk of $\bar{\Omega}$ are necessarily excluded. There is a choice only for the sites in the vicinity of the boundary between Ω and $\bar{\Omega}$ (sites which are both connected to bonds $\in\Omega$ and bonds $\notin\Omega$). The number of possible Λ_i therefore scales as $2^{P(\Omega)}$ where $P(\Omega)$ is the "perimeter" of Ω. Since the calculation of each Pfaffian requires of the order of $\sim N^3$ operations (see Ref. 26 for an explicit algorithm) the computer time required to obtain the RDM (and its spectrum) scales as $\sim N^3 2^{P(\Omega)}$. This method is thus appropriate to study "small" areas in "large" systems. The results of Fig. 10 for zigzag areas with $l_x=8$ and $l_x=10$ were obtained by this method.

The direct enumeration algorithm searches and counts physical dimer configurations one by one for a given set of occupied sites. The enumeration is done separately for Ω and $\bar{\Omega}$, and the required time for each area is almost proportional to the number of dimer coverings, $|\mathcal{E}^i_\Omega|$ or $|\mathcal{E}^i_{\bar{\Omega}}|$. Let $N(\Omega)$ be the number of sites in the "bulk" of Ω, then $|\mathcal{E}^i_\Omega|$ scales as $\sim a^{N(\Omega)}$, where a is a constant. Similarly, $|\mathcal{E}^i_{\bar{\Omega}}|\sim a^{N(\bar{\Omega})}$. Since we have $\sim 2^{P(\Omega)}$ possible Λ_i's, the total computation time adds up to $\sim 2^{P(\Omega)}(a^{N(\Omega)}+a^{N(\bar{\Omega})})$. With the extension of the area Ω, the number of possible Λ_i increases, but counting dimer configurations get faster because $\bar{\Omega}$ shrinks. Thus this method is optimal for large areas in medium-size systems (here up to $N=64$), being complementary to the Pfaffian method. One can reduce the time further by dividing Ω or $\bar{\Omega}$. Let us consider an annulus like in Fig. 4 as Ω, for example. Then $\bar{\Omega}$ can naturally be divided into inner $(r<R_{\text{in}})$ and outer $(r>R_{\text{out}})$ parts, denoted by ω and ω'. Since Ω has two disconnected boundaries, with ω and with ω', one can label $\Lambda(c)$ by two numbers, i and j, corresponding to the occupations around these boundaries. The dimer configurations on ω and ω' can be counted separately for given i and j. The eigenvalues to calculate is therefore expressed as $\lambda_{ij}=|\mathcal{E}^i_\omega|\cdot|\mathcal{E}^{ij}_\Omega|\cdot|\mathcal{E}^j_{\omega'}|/|\mathcal{E}|$. Let P (P') be the "length" of the boundary between Ω and ω (ω'). The required computation time becomes $\sim 2^P a^{N(\omega)}+2^{P+P'}a^{N(\Omega)}+2^{P'}a^{N(\omega')}$. By dividing areas, in general, one can reduce the time of counting configurations in this way, but the number of possible occupations at the boundaries increases. One needs to choose an efficient division, depending on the system and area sizes.

*Present address: Condensed Matter Theory Laboratory, RIKEN, Wako, Saitama 351-0198, Japan

[1] M. Srednicki, Phys. Rev. Lett. **71**, 666 (1993).
[2] C. Holzhey, F. Larsen, and F. Wilczek, Nucl. Phys. B **424**, 443 (1994); G. Vidal, J. I. Latorre, E. Rico, and A. Kitaev, Phys. Rev. Lett. **90**, 227902 (2003); P. Calabrese and J. Cardy, J. Stat. Mech.: Theory Exp. 2004, P06002; N. Laflorencie, E. S. Sorensen, M.-S. Chang, and I. Affleck, Phys. Rev. Lett. **96**, 100603 (2006); S. Ryu and T. Takayanagi, *ibid.* **96**, 181602 (2006).
[3] E. Fradkin and J. E. Moore, Phys. Rev. Lett. **97**, 050404 (2006).
[4] X.-G. Wen and Q. Niu, Phys. Rev. B **41**, 9377 (1990); X.-G. Wen, Phys. Rev. B **44**, 2664 (1991).
[5] X.-G. Wen, *Quantum Field Theory of Many-Body Systems* (Oxford University Press, Oxford, 2004).
[6] L. B. Ioffe and M. V. Feigel'mann, Phys. Rev. B **66**, 224503 (2002).
[7] S. Furukawa, G. Misguich, and M. Oshikawa, Phys. Rev. Lett. **96**, 047211 (2006); J. Phys.: Condens. Matter **19**, 145212 (2007).
[8] S. Furukawa, Ph.D. thesis, Tokyo Institute of Technology, Tokyo, 2007.
[9] J. Preskill, J. Mod. Opt. **47**, 127 (2000).
[10] A. Kitaev and J. Preskill, Phys. Rev. Lett. **96**, 110404 (2006).
[11] M. Levin and X.-G. Wen, Phys. Rev. Lett. **96**, 110405 (2006).
[12] R. Moessner and S. L. Sondhi, Phys. Rev. Lett. **86**, 1881 (2001).
[13] D. S. Rokhsar and S. A. Kivelson, Phys. Rev. Lett. **61**, 2376 (1988).
[14] A. Y. Kitaev, Ann. Phys. (N.Y.) **303**, 2 (2003).
[15] A. Hamma, R. Ionicioiu, and P. Zanardi, Phys. Lett. A **337**, 22 (2005); Phys. Rev. A **71**, 022315 (2005).
[16] G. Misguich, D. Serban, and V. Pasquier, Phys. Rev. Lett. **89**, 137202 (2002).
[17] M. Haque, O. Zozulya, and K. Schoutens, Phys. Rev. Lett. **98**, 060401 (2007).
[18] A. Ioselevich, D. A. Ivanov, and M. V. Feigel'mann, Phys. Rev. B **66**, 174405 (2002).
[19] P. Fendley, R. Moessner, and S. L. Sondhi, Phys. Rev. B **66**, 214513 (2002).
[20] L. B. Ioffe, M. V. Feigel'man, A. Ioselevich, D. Ivanov, M. Troyer, and G. Blatter, Nature (London) **415**, 503 (2002).
[21] A. Ralko, M. Ferrero, F. Becca, D. Ivanov, and F. Mila, Phys. Rev. B **71**, 224109 (2005); *ibid.* **74**, 134301 (2006).
[22] F. J. Wegner, J. Math. Phys. **12**, 2259 (1971).
[23] R. Moessner, S. L. Sondhi, and E. Fradkin, Phys. Rev. B **65**, 024504 (2002).
[24] M. Nielsen and I. L. Chuang, *Quantum Computation and Quantum Information* (Cambridge University Press, Cambridge, 2000).
[25] P. W. Kasteyleyn, Physica (Amsterdam) **27**, 1209 (1961); J. Math. Phys. **4**, 287 (1963); see also Refs. 18 and 19.

[26] O. Derzhko and T. Krokhmalskii, Phys. Status Solidi B **208**, 221 (1998); Y. Maeda and M. Oshikawa, Phys. Rev. B **67**, 224424 (2003).

[27] The zigzag area under consideration is not a disk (the width is too small to contain one unit cell of the $\sqrt{12}\times\sqrt{12}$ crystal) but all the $d=12$ VBC patterns can be distinguished by some appropriate observable defined on this area. We thus expect the same scaling as for disks.

[28] Since the lattices we consider have periodic boundary conditions, four Pfaffians (corresponding to periodic/antiperiodic boundary conditions in both directions) must in fact be combined to get the number of coverings in a given topological sector.